Meteorological, chemical and biological evaluation of the coupled chemistry-climate WRF-Chem model from regional to urban scale. An impact-oriented application for human health

Alessandro Anav [a,1], Beatrice Sorrentino [a,1], Alessio Collalti [b,c], Elena Paoletti [d], Pierre Sicard [e,f], Fatimatou Coulibaly [e], Jacopo Manzini [d], Yasutomo Hoshika [d], Alessandra De Marco [a,f,*]

[a] Italian National Agency for New Technologies, Energy and Sustainable Economic Development (ENEA), Via Anguillarese 301, 00123, Rome, Italy
[b] Forest Modelling Lab., Institute for Agriculture and Forestry Systems in the Mediterranean, National Research Council of Italy (CNR-ISAFOM), Via Madonna Alta 128, 06128, Perugia, Italy
[c] National Biodiversity Future Center (NBFC), 90133, Palermo, Italy
[d] Research Institute on Terrestrial Ecosystems, National Research Council of Italy (IRET-CNR), Via Madonna del Piano 10, 50019, Sesto Fiorentino, Florence, Italy
[e] ARGANS, Sophia Antipolis, France
[f] INCDS, Marin Dracea Institute, Romania

A B S T R A C T

Extreme climatic conditions, like heat waves or cold spells, associated to high concentrations of air pollutants are responsible for a broad range of effects on human health. Consequently, in the recent years, the question on how urban and peri-urban forests may improve both air quality and surface climate conditions at city-scale is receiving growing attention by scientists and policymakers, with previous studies demonstrating how nature-based solutions (NBS) may contribute to reduce the risk of population to be exposed to high pollutant levels and heat stress, preventing, thus, premature mortality. In this study we present a new modeling framework designed to simulate air quality and meteorological conditions from regional to urban scale, allowing thus to assess the impacts of both air pollution and heat stress on human health at urban level. To assess the model reliability, we evaluated the model's performances in reproducing several relevant meteorological, chemical, and biological variables. Results show how our modeling system can reliably reproduce the main meteorological, chemical, and biological variables over our study areas, thus this tool can be used to estimate the impact of air pollution and heat stress on human health. As an example of application, we show how common heat stress and air pollutant indices used for human health protection change when computed from regional to urban scale for the cities of Florence (Italy) and Aix en Provence (France).

1. Introduction

In the recent years, the question on how urban and peri-urban forests may modify both air quality and surface climate conditions within the cities is receiving growing attention by scientists and policymakers (e.g., Sicard et al., 2023a,b; Manzini et al., 2023). In fact, it is well known how the exposure to high concentrations of air pollutants, mainly tropospheric ozone (O_3), nitrogen dioxide (NO_2) and fine particulate matter ($PM_{2.5}$), leads to premature mortality, with millions of people dying every year from cardiovascular and pulmonary diseases caused by exposure to high levels of these pollutants (Zhang et al., 2017). Furthermore, extreme weather events such as heat waves or cold spells are accountable for a wide array of health impacts, spanning from dehydration to heatstroke, and more broadly, exacerbating preexisting cardiovascular and respiratory conditions that could result in fatal outcomes, particularly among the elderly (WHO, 2021). As it is expected that by 2050 nearly 70% of the world's population will live in urban areas, nature-based solutions (NBS) may contribute to reduce the risk of population to be exposed to high pollutant levels and heat stress, preventing, thus, premature mortality (Iungman et al., 2023; Kondo et al., 2020).

Among different removal processes at the Earth's surface, the removal of gases by dry deposition is the main sink for many atmospheric trace gases (e.g., Monks et al., 2015; Clifton et al., 2020). The dry deposition mainly occurs through plant stomata (Paoletti et al., 2019; Sun et al., 2022), i.e., small pores on leaves controlling vapor and gas

---

exchange, but also other plant surfaces (branches, trunks, and canopies) and soil are also able to capture trace gases (Clifton et al., 2020). Dry deposition plays a crucial role in the removal of surface O_3, with stomatal uptake representing a significant component of this process. At global scale, it has been estimated that the annual sink of surface O_3 through dry deposition is 800–900 Tg O_3 yr^{-1} (Hardacre et al., 2015). Plant surfaces also contribute to capture the aerosol, with gravitational settling affecting deposition of particles, especially those larger than a few micrometers in diameter (Wesely and Hicks, 2000). Urban and peri-urban forests not only contribute to capturing air pollutants but also aid in mitigating urban heat island effects. They achieve this by providing shading to building surfaces and streets, deflecting and absorbing radiation from the sun, and releasing moisture into the atmosphere (Akbari et al., 2001).

It has been estimated that shaded surfaces can be 11–25 °C cooler than the maximum temperatures of unshaded materials (Akbari et al., 1997), while the evapotranspiration, combined with shading, can help reduce maximum summer temperatures by 1–5 °C (Akbari et al., 1997; Iungman et al., 2023; Schwaab et al., 2021).

Despite successful legislation on emissions regulation started in the 1990s, a large part of the European population is still exposed to poor air quality, with air pollution levels exceeding both the European standards (Sicard et al., 2021a) and the World Health Organization air quality guidelines for the protection of human health (Sicard et al., 2023a,b). In particular, mainly in the Southern Europe, the warm and sunny climate conditions combined with road traffic, industrial and biogenic emissions promote the O_3 formation (Badia et al., 2023). Consequently, although the stringent regulation, air pollution is still a major environmental concern (Sicard et al., 2023a,b).

In the last decades chemistry transport models (CTMs) have been developed and used to estimate the concentration of gases in atmosphere at global, regional and local scale (e.g. Askariyeh et al., 2020; De Marco et al., 2022). Moreover, CTMs have been used to assess changes in air quality due to different policies of emissions reduction (e.g., Wilson et al., 2012) and assess the capacity of different tree species to absorb gas and particles (e.g., Mircea et al., 2023). Within the AIRFRESH project (LIFE19 ENV/FR/00086), which aims to estimate the air pollution removal capacity of urban forests by planting some selected trees species in two cities, i.e., Florence (Italy) and Aix-en-Provence (France), we have developed a modeling framework which allows simulating air quality from coarse regional scale (i.e., Europe) to urban scale (1 × 1 km) and assess changes in urban air quality and meteorological conditions due to different reforestation strategies. However, before drawing up surveys on the impacts of climate and air pollution on human and ecosystems health, it is important to evaluate how the models simulate the space-time variability of air pollutants and meteorological variables. Several studies already demonstrated how CTMs faithfully reproduce spatial distribution of different chemical species along with their temporal variability (e.g., Karlický et al., 2017; Sicard et al., 2021b). To carefully evaluate the effects of different reforestation strategies, the model should be able not only to reproduce the spatial and temporal variability of meteorological variables, trace gases and aerosols, but also the biological activities related to stomatal conductance, as they affect emissions of Biogenic Volatile Organic Compounds (BVOCs) and deposition of gaseous and particulate pollutants processes.

This paper introduces a numerical approach for simulating meteorological conditions and air quality across regional to local scales, employing the Weather Research and Forecasting model coupled with Chemistry (WRF-Chem) model (Grell et al., 2005). By integrating both meteorological and air quality components within a coupled model framework, consistency is ensured through shared transport schemes, horizontal and vertical grids, and physics schemes for subgrid-scale transport. The primary objective of this study is to evaluate the reliability of various physical, chemical, and biological components within the modeling system and illustrate how this integrated framework can be utilized to assess the impact of air pollutants on human health.

2. Materials and Methods

2.1. Model description

The Weather Research and Forecasting (WRF) model, integrated with atmospheric chemistry capabilities (WRF-Chem), facilitates the comprehensive simulation of trace gas and aerosol dynamics alongside meteorological phenomena (Grell et al., 2005). In this investigation, a nested domain approach was adopted to refine spatial resolution from regional to city scales. Initially, a broad domain (d01) covering Europe was configured with a 15 km horizontal resolution on a Lambert conformal grid. Subsequently, a finer domain (d02) centered on the Western Mediterranean Sea was established at 5 km resolution (see Fig. 1). Finally, air quality simulations were conducted at a 1 km resolution for two urban areas: Florence (Italy) and Aix-en-Provence (France). Vertically, the model utilizes 35 hybrid vertical levels from the surface to 50 hPa. The simulation period corresponds to 2019, representing pre-COVID-19 conditions. Meteorological inputs, including time-varying sea surface temperature, were obtained from the European Centre for Medium-Range Weather Forecasts (ECMWF) ERA5 reanalysis project, with approximately 31 km horizontal resolution every 3 h (Hersbach et al., 2020). Chemical boundary conditions were provided by CAM-Chem, a component of the NCAR-CESM, offering global tropospheric and stratospheric composition data (Tilmes et al., 2015). Anthropogenic emissions were sourced from CAMS-GLOB-ANT data (Soulie et al., 2023), while fire emissions were obtained from the Fire Inventory from NCAR (FINN; Wiedinmyer et al., 2011; 2023), and biogenic emissions were calculated online using the MEGAN model within WRF-Chem (Guenther et al., 2006, 2012). Land cover data were adapted from the CORINE dataset at a 100 m resolution, mapped to MODIS classes for compatibility with WRF preprocessing (Pineda et al., 2004).

The WRF-Chem model provides various physical and chemical schemes for atmospheric simulation. Key physical parameterizations include the RRTM (Rapid Radiative Transfer Model) for radiation (Mlawer et al., 1997), YSU (Yonsei University) for boundary layer processes (Hu et al., 2013), and the Noah-MP Land Surface Model for surface-atmosphere interactions (Li et al., 2022). For atmospheric chemistry, MOZART (Model for OZone And Related chemical Tracers) simulates gas-phase reactions (Emmons et al., 2010), while MOSAIC (Model for Simulating Aerosol Interactions and Chemistry) accounts for aerosol dynamics (Zaveri et al., 2008; Chapman et al., 2009).

2.2. Observational data and site description

Different observational-based datasets are used to evaluate the physical, chemical, and biological components of WRF-Chem. The ability of the WRF-Chem model to reproduce realistic spatio-temporal patterns of relevant surface meteorological variables is assessed by comparing seasonally averaged temperature and precipitation against ERA5-Land reanalysis (Muñoz-Sabater et al., 2021). In addition to spatial patterns, we also computed root mean square error (RMSE) and domain-averaged bias to provide a measure of the model's skills.

To assess the performances of WRF-Chem in reproducing surface NO_2, O_3 and $PM_{2.5}$ mean concentrations, we compared model outputs with in-situ observations from several background monitoring sites belonging to the Airbase network (https://www.eea.europa.eu/en).

Terrestrial plants fix atmospheric carbon dioxide (CO_2) as organic compounds through the photosynthesis process. In addition to the CO_2, required for the photosynthesis, plant leaves can uptake other trace gases through stomata (Paoletti et al., 2019). Like production of organic compounds and deposition of air pollutants are highly correlated (Anav et al., 2018), both depending on stomatal opening, we focused on the validation of the gross primary production (GPP) to assess the reliability of the model in reproducing this biological process. We used both MODIS satellite retrievals (MOD17A2 product; Masuoka et al., 1998)
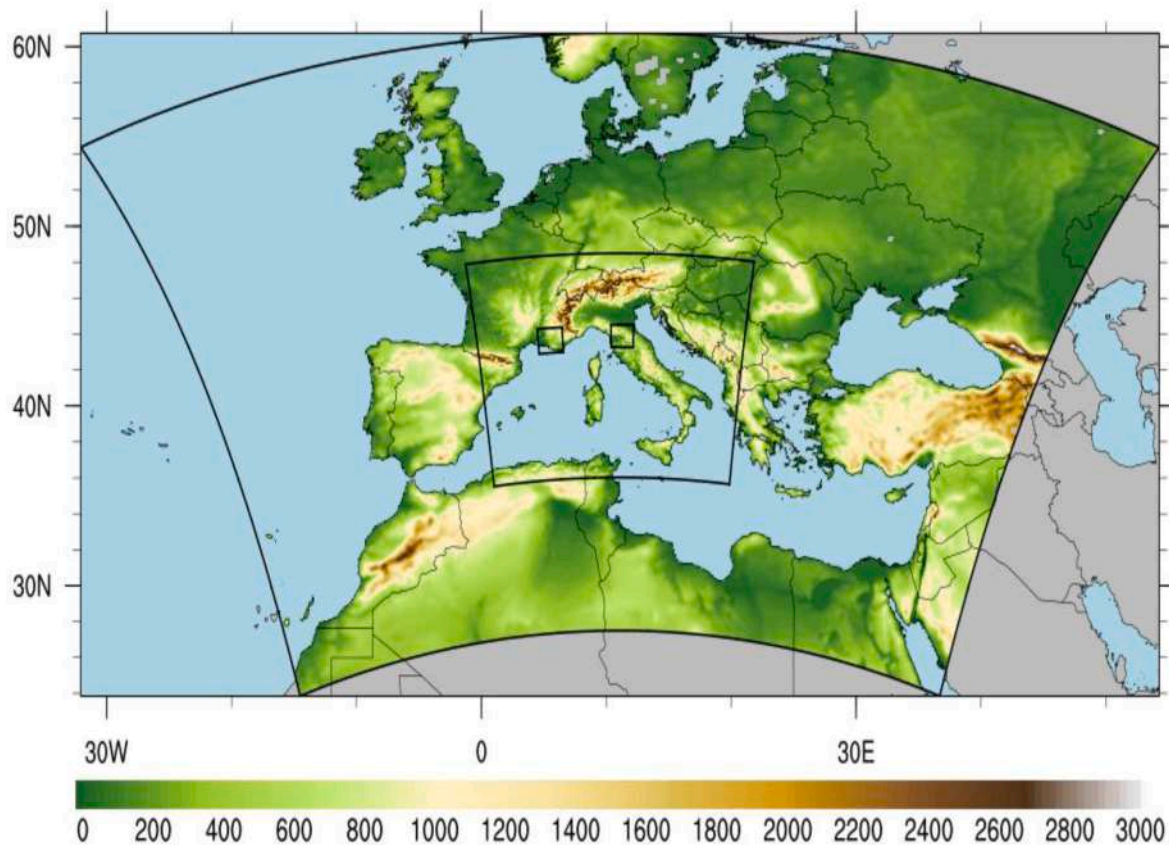
Fig. 1. Domains used for the simulations as defined by the black solid lines. The external European domain (d01) has a horizontal resolution of 15 km, the intermediate Mediterranean domain (d02) has a resolution of 5 km, while urban domains over Florence and Aix en Provence have a resolution of 1 km.

and in-situ eddy covariance data (Pastorello et al., 2020) coming from 12 monitoring stations (Table 1), representative of the main European vegetation types, from the ICOS Ecosystem station network (http s://www.icos-cp.eu/): Evergreen needleleaf forests (Davos, Bilos, Puechabon, Hyltemossa, Norunda), Grasslands (Grillenburg, Torgnon), Deciduous broadleaf forests (Hainich, Hohes Holz, Fontainebleau-Barbeau), Croplands (Klingenberg) and Open shrublands (Lison), respectively.

2.3. O_3 exposure and thermal stress indices for human health

Ozone exposure relevant to health impacts is quantified using the Sum of Ozone Means Over 35 ppb (SOMO35). Worldwide, this metric is widely used to assess the health impact of ozone exposure, as recommended by the World Health Organization (WHO). It represents the yearly cumulative total of daily maximum 8-h running average ozone concentrations that exceed 35 ppb (parts per billion), over the entire year (Paoletti et al., 2007; Malley et al., 2015).

Similarly, to quantify the thermal stress to human health, we computed the Universal thermal climate index (UTCI) (e.g. Martilli et al., 2023; Di Napoli et al., 2018); it is a human biometeorological parameter used to assess the relationship between the external environment and human well-being. This index quantifies the combined effects of temperature, wind, radiation, and humidity on the interaction between the human body and the surrounding thermal environment. Further details can be found into Martilli et al. (2023)

3. Results and discussion

3.1. Validation of meteorological variables

Considering the surface air temperature (Fig. 2), WRF-Chem displays, in all the seasons, a fairly good agreement with the reanalysis in both the parent and nested domains, with a typical meridional gradient and notably lower air temperatures over the Alps, Pyrenees and Carpathian mountains than the flatter continental Europe. Looking at the mean bias (Table 2), results highlight a minimal underestimation of the 2 m temperature during winter (−0.27 and −0.13 °C for d01 and d02, respectively) and a minimal overestimation during summer months (0.19 and 0.52 °C for d01 and d02, respectively), while the largest bias, occurring during spring, is systematically lower than 1 °C in both the domains (0.4 and 0.8 °C).

Compared to other studies performed with the same regional climate model over Europe (e.g., Mooney et al., 2013; Katragkou et al., 2015), our simulations show better performances in reproducing the surface air temperature. In particular, the cold bias occurring in North-Eastern Europe during winter, exceeding the 8 °C in some configurations (Mooney et al., 2013), does not appear in our results. Similarly, the summer warm bias, exceeding 5 °C over the whole continental Europe (Mooney et al., 2013), noticeably decreased in magnitude in our simulations.

In addition to the mean seasonal cycle, Fig. S1 suggest how the model correctly reproduces the diurnal variability of temperature, over the prudence sub-regions (Christensen and Christensen, 2007), during both winter and summer.

Besides to surface air temperature, we compared the mean seasonal precipitation computed by WRF-Chem against ERA5-Land reanalysis (Fig. 3). Although in the European domain the location of maximum
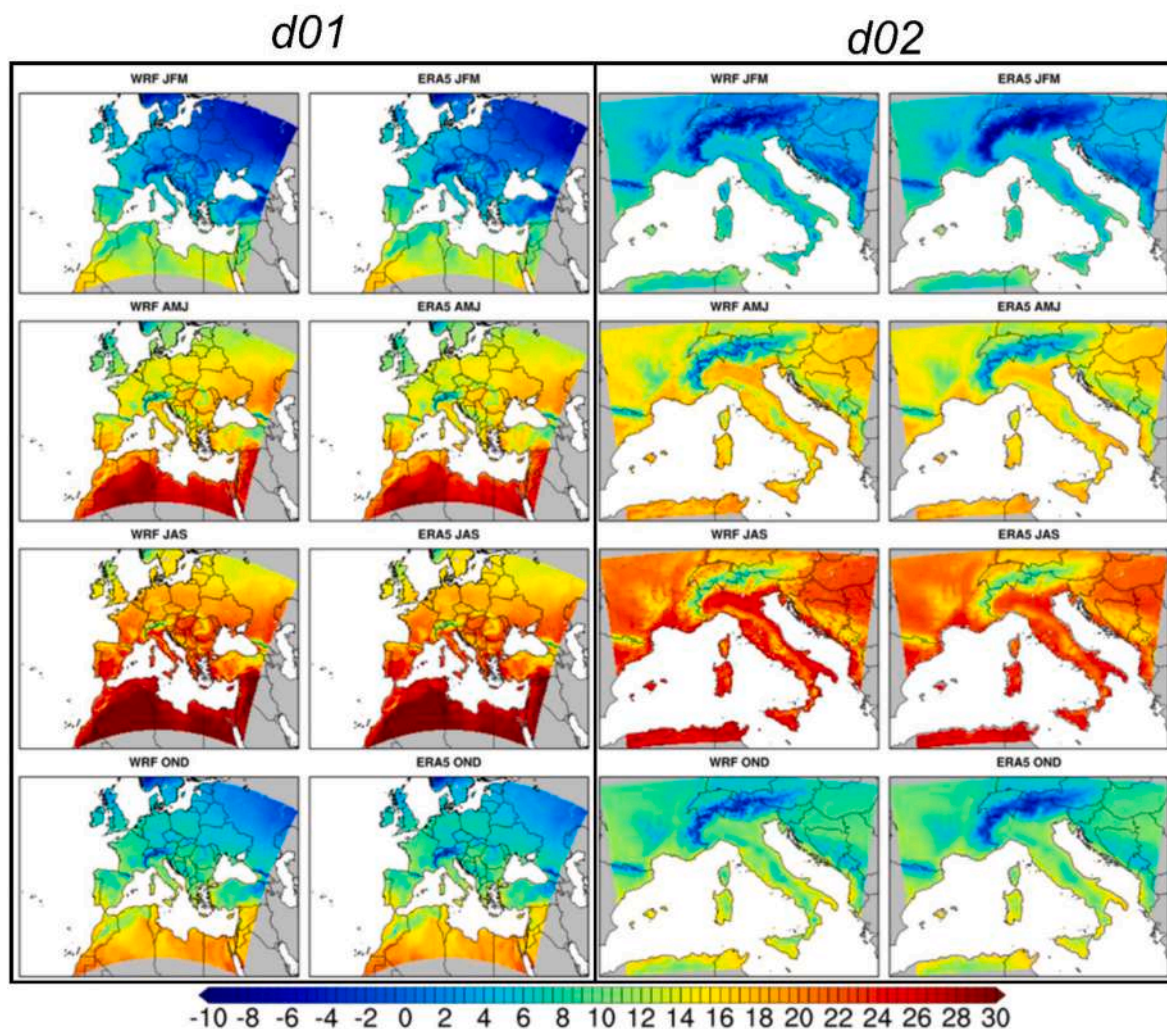
Fig. 2. Mean seasonal mean near-surface air temperature (°C) as simulated by WRF-Chem and ERA5-Land over European domain (d01) and Mediterranean domain (d02) for boreal winter JFM (January-February-March), spring AMJ (April-May-June), summer JAS (July-August-September), and autumn OND (October-November-December).

precipitation is in agreement between WRF-Chem and ERA5-Land, WRF-Chem remarkably underestimates land precipitation during all the seasons, with the most pronounced dry bias (-0.52 mm day^{-1}) occurring during fall (Table 2). In addition to a more resolved pattern around the mountains, the nested domain over the Western Mediterranean Sea does not show any relevant underestimation of precipitation, and the bias is lower than its parent domain. The effect of aerosols in the formation of condensation nuclei as well as their effects on cloud cover and precipitation are widely known (Alma and Knote, 2014; Brasseur and Roeckner, 2005; Menon, 2004). As aerosols have a substantial impact on the hydrogeological cycle (Wu et al., 2013), the dry bias found in the parent domain could be due to differences in the time-varying aerosols used by ERA5-Land and those simulated by WRF-Chem.

3.2. Validation of chemical variables

Fig. 4 shows the seasonal averages concentrations for NO_2 as simulated by WRF-Chem and in-situ measurements provided by European Environment Agency database (EEA). Overall, we found a general good agreement between model results and observations in all the seasons and domains, with results of Table 3 highlighting a systematic underestimation of NO_2 both in the parent and nested domain, with the largest bias occurring over the Mediterranean domain during winter (-9 ppb).

Despite the general good agreement with in-situ measurements, in some urban sites there is a large mismatch likely due to the poorly reproducibility of urban air quality because of the coarse resolution of our domains, i.e., 15 and 5 km, respectively (Tuccella et al., 2012). In addition, the lack of local emission inventories does not allow to capture the local scale variability, especially in the cities. This is confirmed by several studies which demonstrated how increasing the spatial resolution of the anthropogenic emission inventory can help WRF-Chem to better capture the local variability of air pollutants (e.g. Zhong et al., 2016; López-Noreña et al., 2022).

As the NO_2 concentrations are directly linked to non-industrial combustion, road traffic and other mobile source emissions, the highest concentrations are located over urban areas and along ship tracks. Fig. 4 shows how the model correctly reproduces this pattern with the higher NO_2 concentrations observed over the densely populated European cities (e.g., London, Paris) as well as in the major Italian cities such as Milan, Turin, Rome and Naples, and in the whole Po Valley, where the atmospheric inversion, taking place during winter and fall, contributes to the stagnation of air masses making this region one of the most polluted areas of Italy (Petritoli et al., 2003). Besides, the main ship tracks of Mediterranean Sea and Atlantic Ocean are clearly visible.

Considering the O_3, during cold period it is characterized by decreasing concentrations due to NO_x titration, while during warm
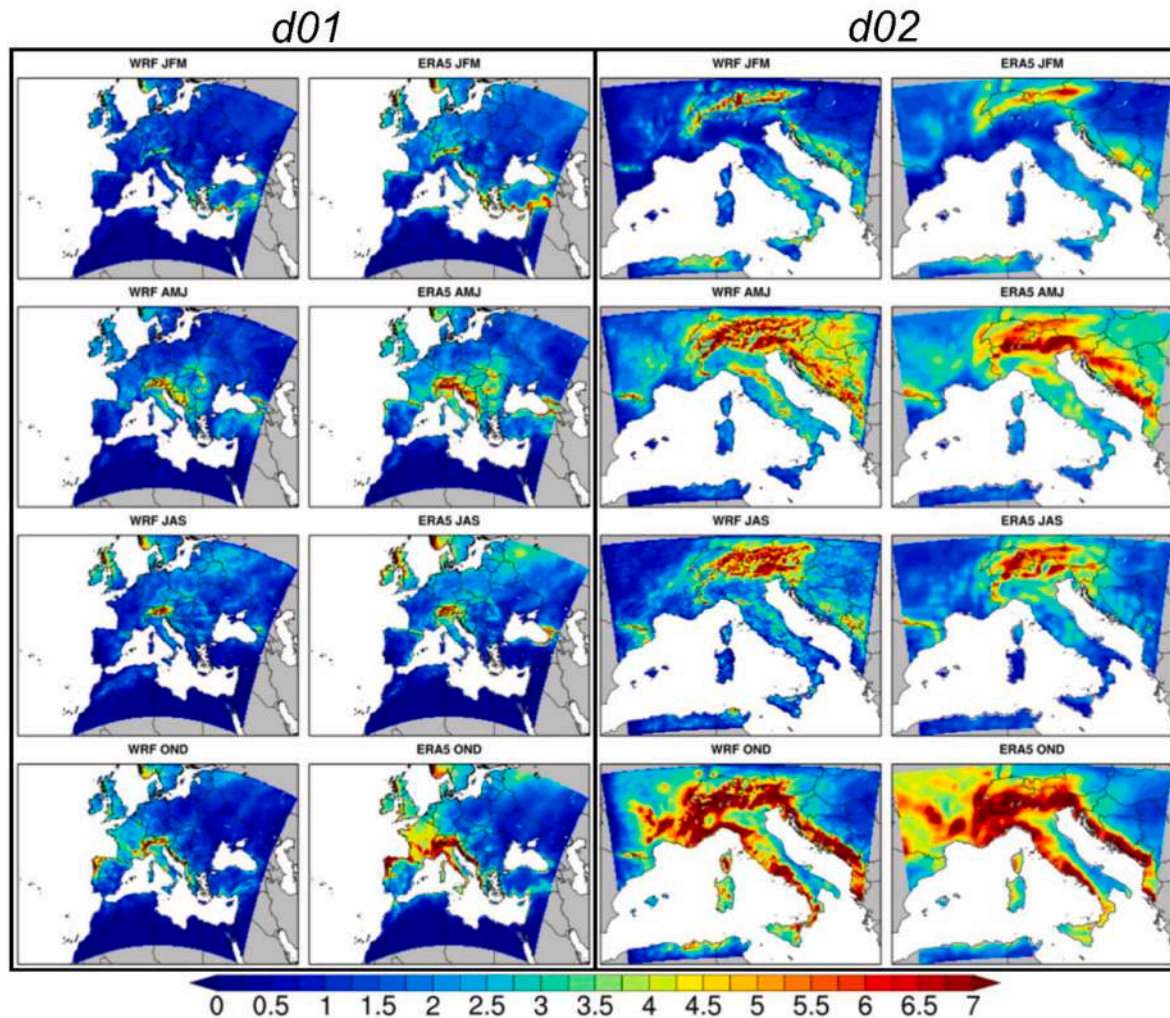
Fig. 3. Precipitation (mm day^{-1}) as simulated by WRF-Chem and ERA5-Land over European domain (d01) and Mediterranean domain (d02) for boreal winter JFM (January-February-March), spring AMJ (April-May-June), summer JAS (July-August-September), and autumn OND (October-November-December).

periods the higher photolysis rates promote the O_3 formation (Monks et al., 2015; Sicard et al., 2016). In addition, over the Mediterranean Sea the lower dry deposition rates and lower boundary layer heights lead to higher concentrations (Terrenoire et al., 2015; Sicard et al., 2016). The model well reproduces the expected seasonal variability as well as the spatial pattern, this latter characterized by higher concentrations in the south-east part of the domain, reaching up to 52 ppb during winter and more than 60 ppb during summer (Fig. 5). Compared to in-situ data, in general WRF-Chem overestimates the observations near the major European cities with the largest mismatch observed in the southern regions of our study area. The largest biases are found during fall both for the parent (9.6 ppb) and nested (14.6 ppb) domains. This overestimation of O_3 concentrations by WRF-Chem may be partly linked to the underestimation of NO_2 but could also be due to the condition of the monitoring stations which are at lower height than the first model layers. Another possible explanation for the overestimation of O_3 may be due to the common underestimation of the volatile organic compound (VOC) emissions. The discrepancy between the predicted concentrations of O_3 and NO_2, where O_3 tends to be overestimated and NO_2 tends to be underestimated throughout the year, may be attributed to several factors. According to Zhang et al. (2017), one contributing factor could be the inadequate titration of O_3 by NO, resulting in an overestimation of O_3 levels and an underestimation of NO_2 levels.

During warmer periods when plant activity is heightened, the WRF-Chem model tends to overestimate surface O_3 concentrations. This discrepancy can be partially explained by two main factors. Firstly, Wu et al. (2013) suggest that the model may inadequately parameterize dry deposition to vegetation, leading to underestimated dry deposition velocities. Consequently, this reduces the capacity of plants to remove O_3 from the atmosphere. Secondly, Ryu et al. (2018) propose that the model's underestimation of cloud optical depth and overestimation of photolysis rates could further contribute to the discrepancy, exacerbating the overestimation of O_3 concentrations. Fig. 6 shows how $PM_{2.5}$ concentrations are well reproduced by the model in both the parent and nested domains. Highest concentrations are observed during colder seasons (i.e. winter and fall) because of the combustions of domestic heating systems, such as wood or pellet stoves, which emit particles into the air (Perrino et al., 2019). Furthermore, during winter, temperature inversion can cause an accumulation of fine particles in the air (Nidzgorska-Lencewicz et al., 2020), as clearly visible in the norther part of Italy (Po Valley) where stable meteorological conditions associated to vehicular traffic, industry, agriculture and domestic use of fossil fuels emission promote the formation of $PM_{2.5}$ (Fig. 6). The model generally overestimates the $PM_{2.5}$ concentrations in all the domains (from about 3 µg m^{-3} to 5 µg m^{-3}), except in JFM where the model tends to slightly underestimate (from about -1.15 µg m^{-3} to -2 µg m^{-3}) the $PM_{2.5}$ (Table 3). The largest bias, corresponding to about 5 µg m^{-3} are found during fall. These results are consistent with other evaluation and
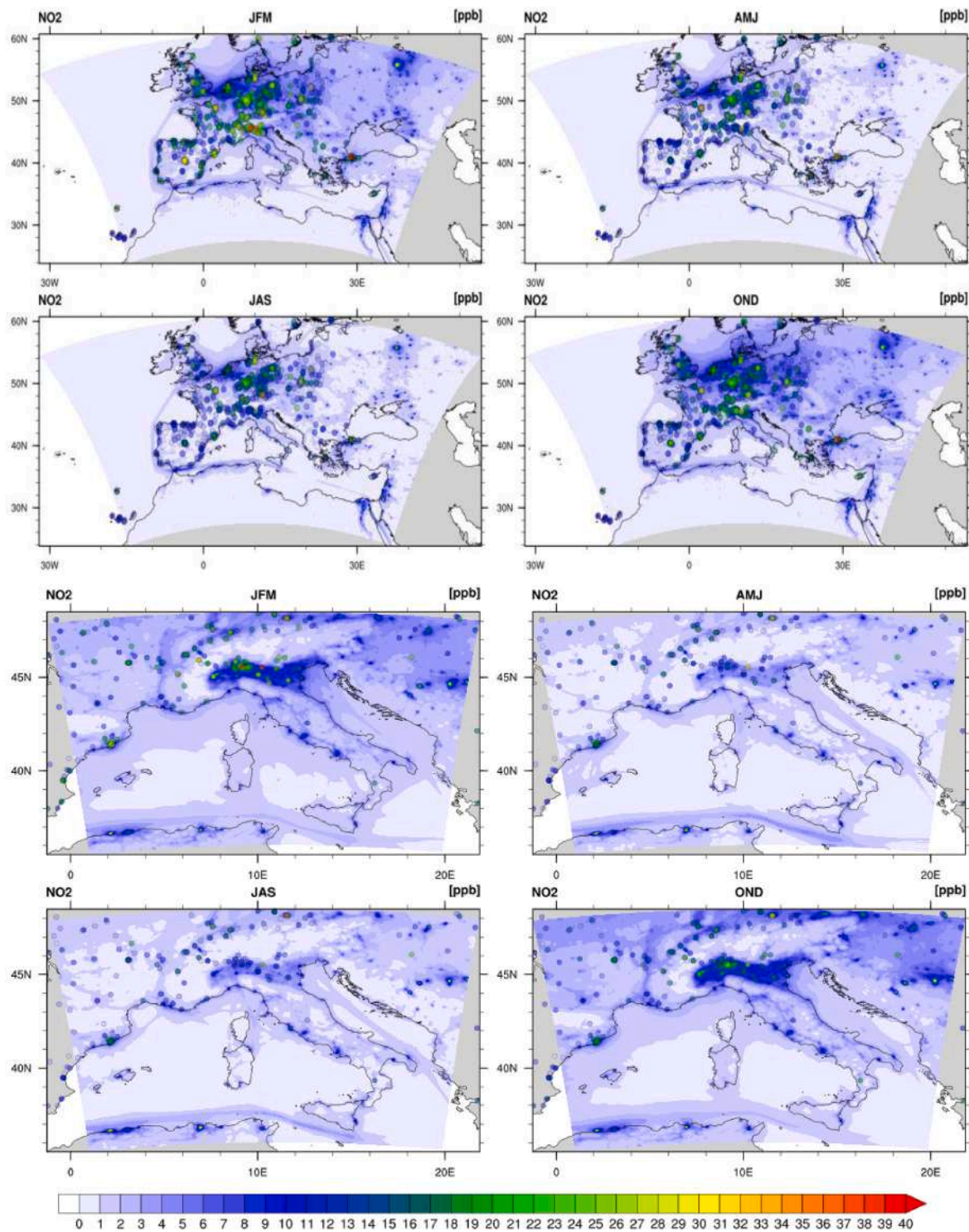
Fig. 4. Seasonal averages concentrations for NO$_2$ [ppb] modeled by WRF-Chem for the European domain overlapped by measurement stations (dots).

sensitivity studies of WRF-Chem over Europe (Stern et al., 2008; Tuccella et al., 2012) which showed biases ranging from −13.50 μg m^{-3} to +7.64 μg m^{-3}.

In addition to mean seasonal averages, in Fig. S2 we also present the validation of the mean winter (PM2.5 and PM10) and summer (NO2 and O3) daily cycle as simulated by WRF-Chem and measured through the Airbase network.

3.3. Validation of main biological variables

Total annual GPP maps, for the year 2019, are shown in Fig. 7, as simulated by WRF-Chem and compared with satellite observations (i.e., MODIS). Results suggest that WRF-Chem is generally able to capture the observed GPP spatial distribution, with a good spatial correlation of 0.97 for both domains. However, results also display a large underestimation (>200 gC m^{-2} y^{-1}) of the GPP peak, mostly in the parent domain. The underestimation of the peak in the GPP affects the total spatial integral, which is 9.4 PgC for WRF-Chem and 9.7 PgC for MODIS in the parent
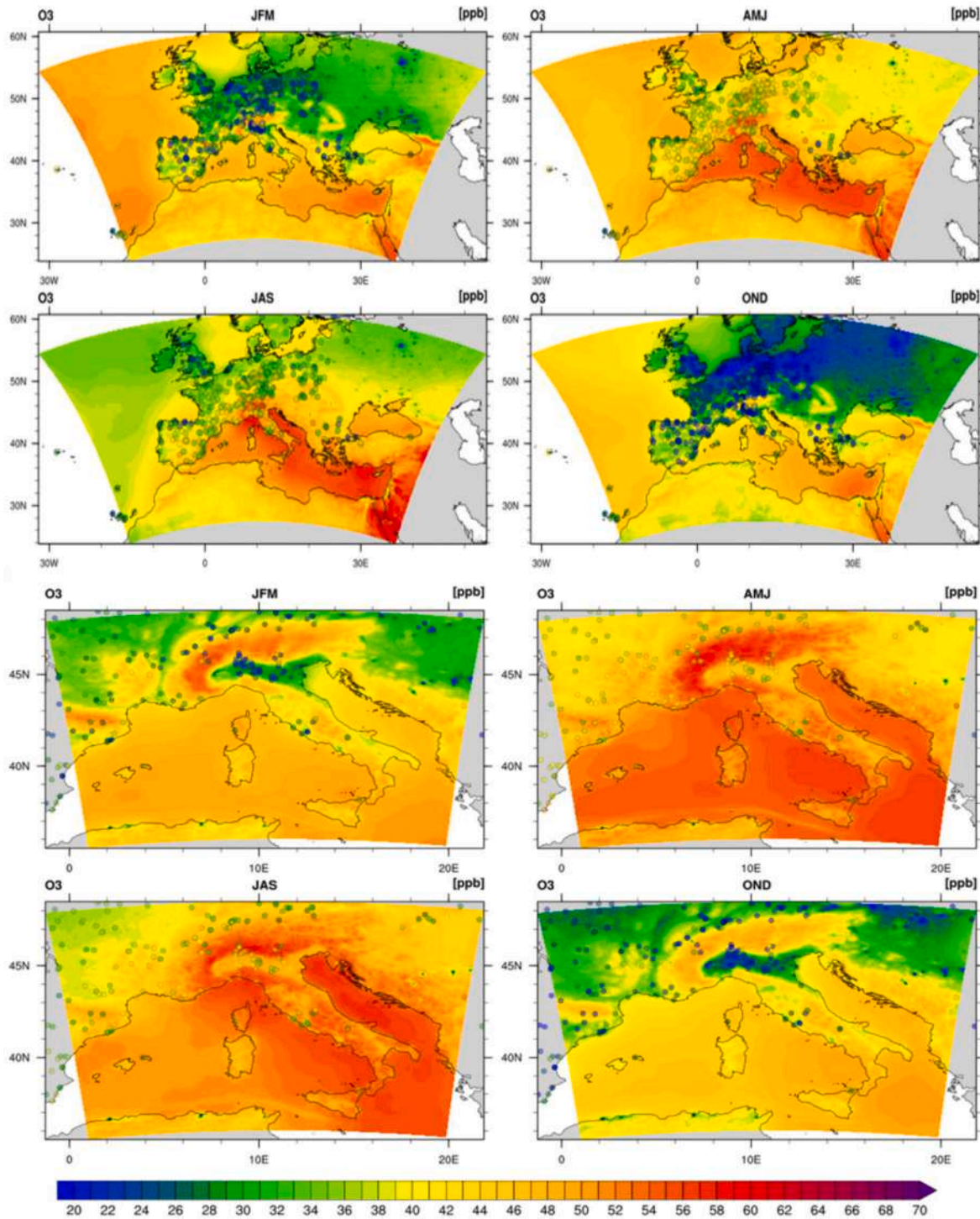
Fig. 5. Seasonal averages concentrations for O₃ [ppb] modeled by WRF-Chem for the European domain overlapped by measurement stations (dots).

domain, and 1.8 PgC and 2.0 PgC in the nested domain. However, it should also be considered that MODIS tends to overestimate the GPP (up to 20–30%) when compared to flux tower data (e.g., Wang et al., 2017; Dalmonech et al., 2024). The reasons rely on the overestimation of the fractional photosynthetically active radiation (FPAR): being satellite-based GPP computed from a light use efficiency (LUE) approach, the photosynthesis does not saturate at increasing FPAR, but increases linearly at increasing radiation.

Therefore, to better characterize the simulated GPP and assess how

well the timing of the beginning (budbreak) and the end (leaf fall) of the growing season are reproduced, we present the annual GPP cycle as represented by WRF-Chem and measured over different forest sites across Europe (Fig. 8). Considering the European deciduous forest, at mid-latitude the growing season generally starts in April (CLRTAP, 2017) with the leaf-out, and, consequently, the photosynthetic activity begins to rise (Fig. 8). Then, the GPP reaches its maximum value in July and starts to decrease thereafter because of scarce soil water availability (Peng et al., 2021). In fall, leaves start to fall-out and photosynthetic
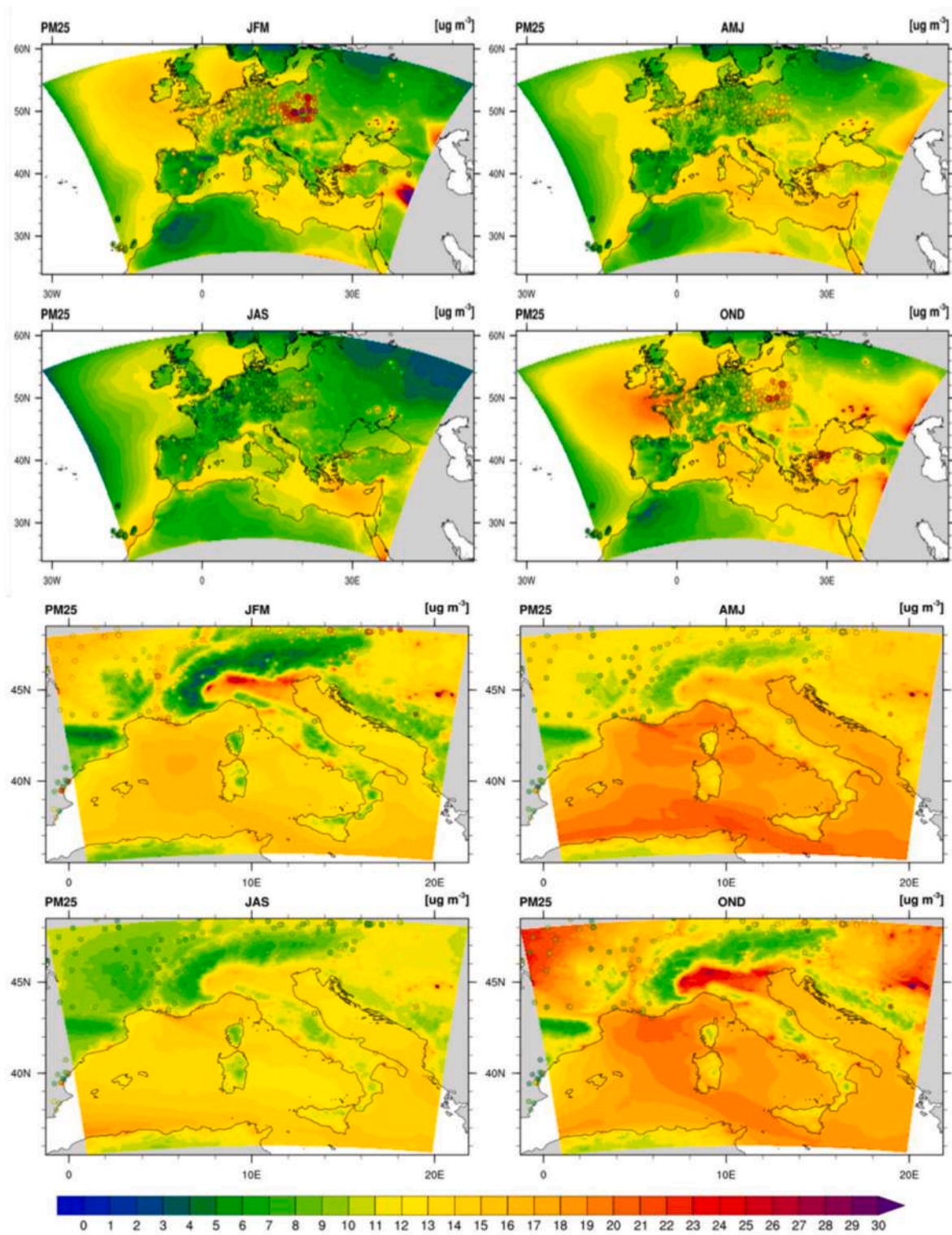
Fig. 6. Seasonal averages concentrations for $PM_{2.5}$ [µg m^{-3}] modeled by WRF-Chem overlapped by measurement stations (dots).

absorption of CO_2 gradually decreases. This pattern is well captured in the three beech sites (DE-Hai, DE-Hoh and FR-For), although in DE-Hai and DE-Hoh the model simulates earlier onset and senescence dates compared to eddy covariance data. In contrast, in FR-For the model has a good agreement with measurement both in terms of the timing of phenological events and amplitude of seasonal cycle. In the sites where evergreen trees are the dominant vegetation, WRF-Chem shows different responses. In particular, in CH-Dav the model is not able to

reproduce both the observed seasonal cycle and amplitude; this seems to be more likely related to differences in the representation of land cover types in this complex mid-mountain area (Bo et al., 2022) rather than to the poor representation of physical or biological processes. This is partially confirmed by the performances of the model in the other evergreen sites, where WRF-Chem shows a remarkable agreement with eddy covariance data in SE-Nor and FR-Pue and a slight underestimation of summer GPP peak in SE-Htm, while in FR-Bil, except during fall, the
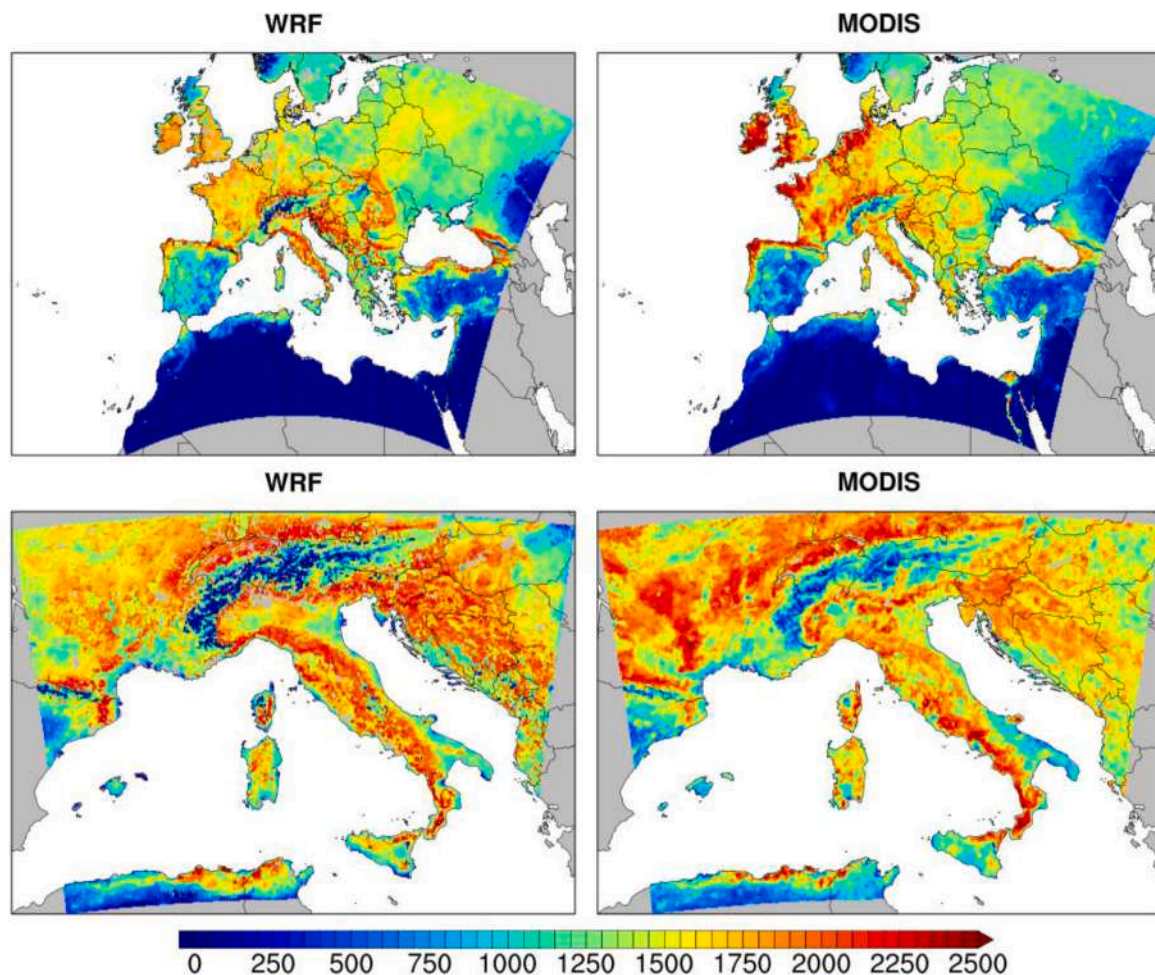
Fig. 7. Annual gross primary productivity (GPP) [gC m^{-2}y^{-1}] for 2019 simulated with WRF-Chem compared with MODIS dataset for the European domain (upper boxes) and Western Mediterranean Sea domain (bottom boxes).

model systematically underestimates the GPP, although the seasonal cycle is well reproduced. Besides, it is worth noting how well the model reproduces the typical heat stress and drought conditions of FR-Pue, characterized by a sharp GPP reduction during the beginning of the summer followed then by a secondary GPP peak at the beginning of the autumn. Considering the shrubland site, WRF-Chem shows a good agreement with eddy covariance data, despite it predicts a remarkable high GPP values during spring, as it does in IT-Tor too. Finally, in DE-Gli there is a strong agreement with measurements despite the sudden GPP drop observed at the end of May and June is not apparently captured by the model. Nonetheless, as highlighted in earlier research by Martinez et al. (2019), the dynamics of this site are significantly shaped by management practices, notably the grassland being harvested two to four times annually, a factor not currently considered by the model. This oversight helps elucidate the sudden decline observed in GPP.

3.4. Human health protection indicators from regional to city-scale

The previous analysis helps to assess the performances of the model in reproducing different meteorological, chemical and biological variables. In this section, as possible application of our modeling framework, we present how common heat stress and air pollutant indices, used for human health protection, change when computed from regional to urban scale for the cities of Florence (Italy) and Aix en Provence (France).

To assess the impact of O$_3$ on human health, according to the World Health Organization (WHO), we use the SOMO35 (see Materials and

Methods). Considering the SOMO35 (Fig. 9, panel A), because of the coarse resolution the parent domain shows homogeneous SOMO35 levels, while the kilometer-scale simulation displays a detailed spatial fragmentation.

Looking at the thermal stress, in Fig. 9 (panel B) we present the UTCI computed as the summer mean (JJA) of daily maxima. In the parent domain the heat stress has a clear latitude gradient, with UTCI values generally increasing towards the south. The intermediate Mediterranean domain is characterized by high insolation patterns and temperatures except over the mountainous regions, with UCTI reflecting this pattern. In the kilometer-scale simulations, around the two analyzed municipalities the UTCI shows values ranging between Strong and Very Strong Heat, highlighting the relevance of such indicator in determining heat-related mortality in Mediterranean region.

4. Conclusions

We presented a modeling framework designed to simulate air quality from regional to urban scale and assess the impacts of air pollution and thermal stress on human health at city-scale. To assess the model reliability, we evaluated its performances in reproducing several relevant meteorological, chemical, and biological variables. Results showed that the WRF-Chem model simulates satisfactory well the main spatio-temporal characteristics of the analyzed meteorological variables. Considering the surface air temperature, the mean bias ranged from −0.27 °C to +0.40 °C in the European domain and from −0.13 °C to +0.79 °C in the nested domain. Compared to other simulations
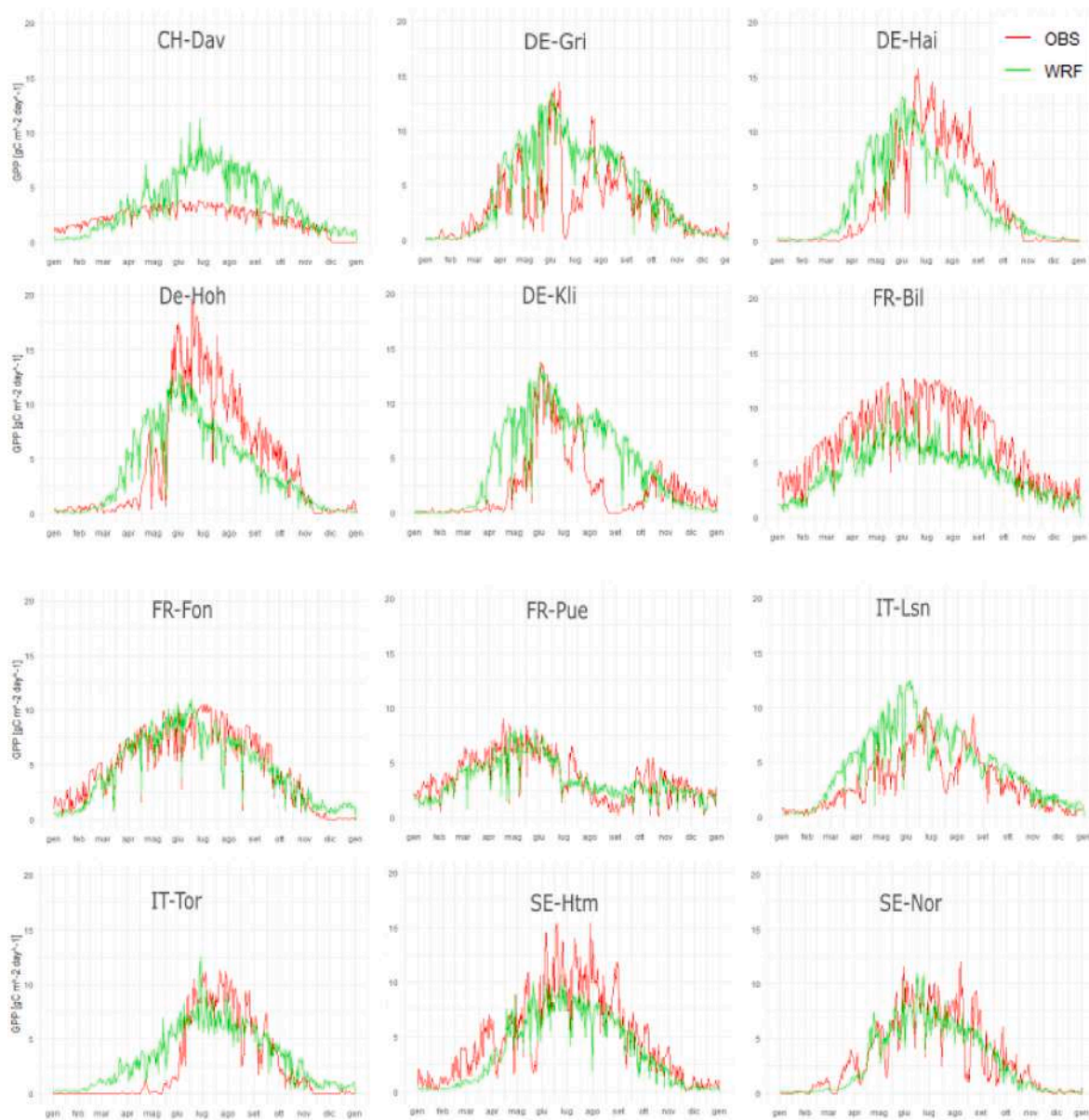
Fig. 8. The WRF-Chem simulated monthly cycle of GPP [gC m^{-2}d^{-1}] (green line) against tower-derived values across the 12 selected sites (red line).

performed over the same region we found a substantial reduction in the well-known winter and summer bias (Mooney et al., 2013). Similarly, the precipitation is in good agreement with previous studies (e.g., Katragkou et al., 2015), although locally some large biases, related to the aerosols-radiation-precipitation feedback, still emerge. In this case, the mean bias ranges from −0.52 mm day^{-1} to +0.44 mm day^{-1} in the European domain and from −0.04 mm day^{-1} to −0.40 mm day^{-1} in the nested domain.

Considering the main trace-gases, despite an underestimation of NO$_2$ and overestimation of O$_3$ concentration mainly over the main European cities, the model is able to correctly reproduce their spatial and temporal variability. Stations located into large cities or close to traffic roads often record very high concentrations of pollutants which cannot be reproduced by the atmospheric model (Sicard et al., 2021b, c), unless it is properly fed with local emission inventories. For instance, Georgiou et al. (2018), comparing WRF-Chem simulated NO$_2$ concentrations with a local station close to a large highway which was not captured by the anthropogenic emission inventory, showed how the high NOx concentrations, resulting from traffic, were not correctly simulated by the model. In a study by López-Noreña et al. (2022), it was demonstrated

that aggregating coarse anthropogenic emissions within a city results in the model producing a sizable and uniform pollutant plume that gradually dissipates towards suburban regions. Conversely, when the emission inventory incorporates detailed spatial data, the model reveals distinct local pollution hotspots and spatial patterns that align with specific emission sources and highway networks (López-Noreña et al., 2022). Despite, the limitations arising from the lack of local emission inventories, the PM$_{2.5}$ concentrations are well simulated in both the domains.

The GPP comparison with satellite data revealed a fair agreement with observation and a general underestimation of the maxima. Nevertheless, it is well known how the satellite-based data tend to overestimate the GPP maxima (Zhu et al., 2023). On the other side, the comparison with in-situ measurements showed a good agreement on both the timing of phenological events and magnitude of GPP in most of the sites. Results highlighted how the model simulates earlier leafing-out in the spring in some sites; this result is consistent with Ma et al. (2017) who showed earlier beginning of the growing season over several sites located in central and eastern areas of continental United States.

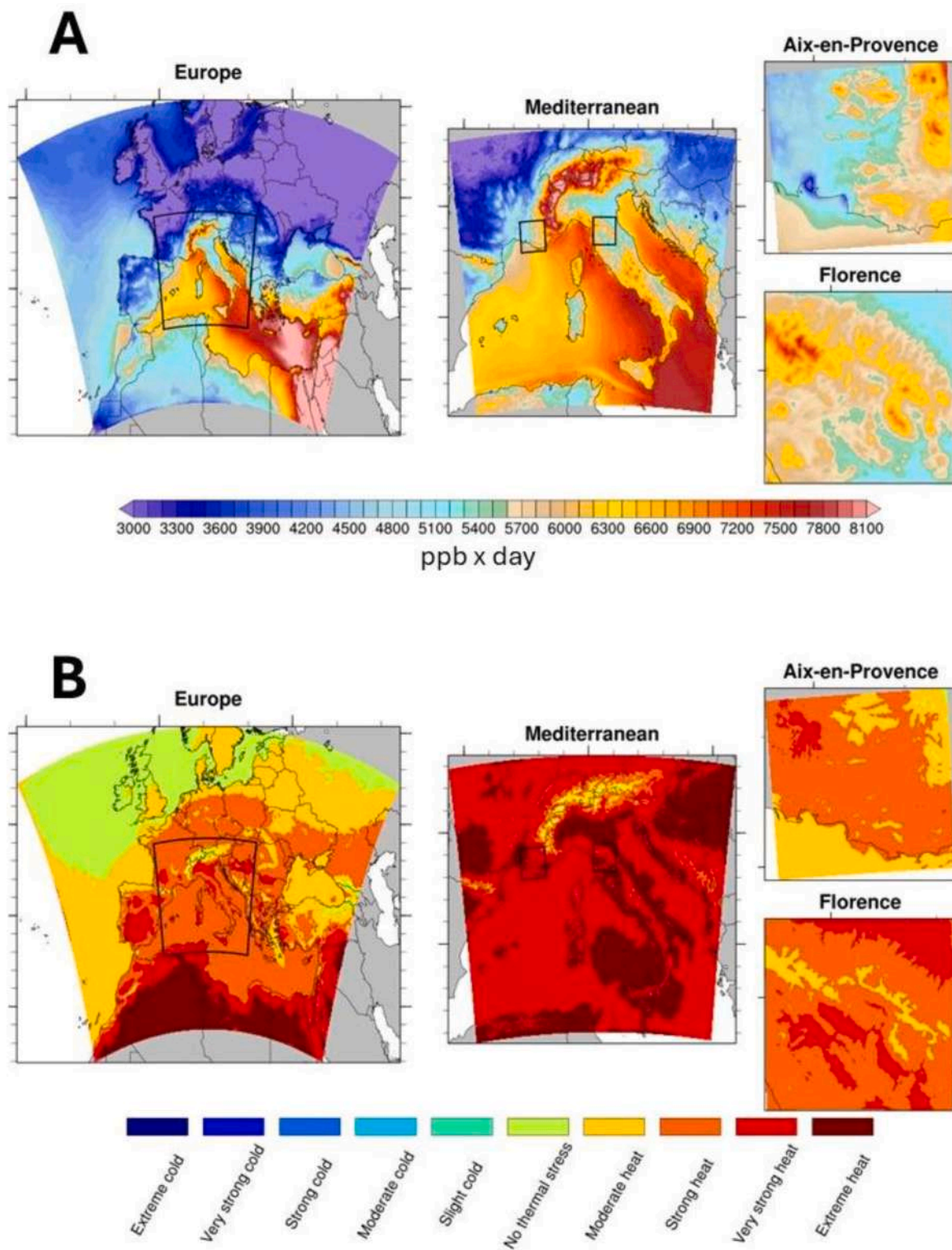Overall, the model validation revealed how the WRF-Chem is able to

Fig. 9. Maps of SOMO35 (upper panel) and thermal heat stress (UTCI, lower panels) over the different domains as simulated by WRF-Chem for the year 2019.

reliably reproduce the main meteorological, chemical, and biological variables over our study areas, therefore model output can be used to feed urban domains without introducing large biases through the boundary conditions.

To conclude, this work showed how results from this modeling framework can be used to estimate the impact of both air pollution and meteorological conditions on human health. As climate change and poor air quality are expected to be a primary cause of death in the next future our approach could be applied to other cities to quantify present and future impacts on health effects of climate change and air pollution. This could potentially allow to identify concrete adaptation measures, especially for the most vulnerable cities.

CRediT authorship contribution statement

Alessandro Anav: Writing – original draft, Methodology, Data curation. **Beatrice Sorrentino:** Writing – original draft, Methodology, Data curation. **Alessio Collalti:** Writing – review & editing, Resources. **Elena Paoletti:** Writing – review & editing, Conceptualization. **Pierre Sicard:** Writing – review & editing, Resources. **Fatimatou Coulibaly:** Validation, Data curation. **Jacopo Manzini:** Writing – review & editing. **Yasutomo Hoshika:** Writing – review & editing. **Alessandra De Marco:** Writing – review & editing, Supervision, Resources, Conceptualization.

Declaration of competing interest

The authors declare that they have no known competing financial interests or personal relationships that could have appeared to influence the work reported in this paper.

Data availability

Data will be made available on request.

Appendix A. Supplementary data

Supplementary data to this article can be found online at https://doi.org/10.1016/j.envres.2024.119401.

References

Akbari, H., Kurn, D.M., Bretz, S.E., Hanford, J.W., 1997. Peak power and cooling energy savings of shade trees. Energy Build. 25 (2), 139–148. https://doi.org/10.1016/S0378-7788(96)01003-1. ISSN 0378-7788.

Akbari, H., Pomerantz, M., Taha, H., 2001. Cool surfaces and shade trees to reduce energy use and improve air quality in urban areas. Sol. Energy 70 (3), 295–310. https://doi.org/10.1016/S0038-092X(00)00089-X. ISSN 0038-092X.

Alma, H., Knote, C., 2014. WRF-Chem 3.6.1: MOZART gas-phase chemistry with MOSAIC aerosols. NCAR/ACD 9.

Anav, A., Liu, Q., De Marco, A., Proietti, C., Savi, F., Paoletti, E., Piao, S., 2018. The role of plant phenology in stomatal ozone flux modeling. Global Change Biol. 24 (1), 235–248. https://doi.org/10.1111/gcb.13823. Epub 2017 Aug 17. PMID: 28722275.

Askariyeh, M.H., Khreis, H., Vallamsundar, S., 2020. Chapter 5 - air pollution monitoring and modeling. In: Khreis, Haneen, Nieuwenhuijsen, Mark, Zietsman, Josias, Ramani, Tara (Eds.), Traffic-Related Air Pollution. Elsevier, pp. 111–135. https://doi.org/10.1016/B978-0-12-818122-5.00005-3. ISBN 9780128181225.

Badia, A., Vidal, V., Ventura, S., Curcoll, R., Segura, R., Villalba, G., 2023. Modelling the impacts of emission changes on O3 sensitivity, atmospheric oxidation capacity, and pollution transport over the Catalonia region. Atmos. Chem. Phys. 23, 10751–10774. https://doi.org/10.5194/acp-23-10751-2023.

Bo, Y., Li, X., Liu, K., Wang, S., Zhang, H., Gao, X., Zhang, X., 2022. Three decades of gross primary production (GPP) in China: variations, trends, attributions, and

prediction inferred from multiple datasets and time series modeling. Rem. Sens. 14 (11), 2564. https://doi.org/10.3390/rs14112564.

Brasseur, G.P., Roeckner, E., 2005. Impact of improved air quality on the future evolution of climate. Geophys. Res. Lett. 32, L23704 https://doi.org/10.1029/2005GL023902.

Chapman, E.G., Gustafson, Jr.W.I., Easter, R.C., Barnard, J.C., Ghan, S.J., Pekour, M.S., Fast, J.D., 2009. Coupling aerosol-cloud-radiative processes in the WRF-Chem model: investigating the radiative impact of elevated point sources. Atmos. Chem. Phys. 9, 945–964. https://doi.org/10.5194/acp-9-945-2009.

Christensen, J.H., Christensen, O.B., 2007. A summary of the PRUDENCE model projections of changes in European climate by the end of this century. Climatic Change 81, 7–30.

Clifton, O., Fiore, A.M., Massman, W.J., Baublitz, C.B., Coyle, M., Emberson, L., Fares, S., Farmer, D.K., Gentine, P., Gerosa, G., et al., 2020. Dry deposition of ozone over land: processes, measurement, and modeling. Rev. Geophys. 58, e2019RG000670.

Dalmonech, D., Vangi, M. Chiesi, Chirici, G., Fibbi, L., Giannetti, F., Marano, G., Massari, C., Nolè, A., Xiao, J., Collalti, A., 2024. Regional estimates of gross primary production applying the Process-Based Model 3D-CMCC-FEM vs. Remote-Sensing multiple datasets. European Journal of Remote Sensing 57, 1. https://doi.org/10.1080/22797254.2023.2301657.

De Marco, A., Héctor, G.-G., Collalti, A., Omidi Khaniabadi, Y., Proietti, C., Sicard, P., Vitale, M., Anav, A., Paoletti, E., 2022. Ozone modelling and mapping for risk assessment: an overview of different approaches for human and ecosystems health. Environ. Res. 211 https://doi.org/10.1016/j.envres.2022.113048.

Di Napoli, C., Pappenberger, F., Cloke, H.L., 2018. Assessing heat-related health risk in europe via the universal thermal climate index (UTCI). Int. J. Biometeorol. 62, 1155–1165. https://doi.org/10.1007/s00484-018-1518-2.

EEA, 2022. Report no. 05/2022 Title: Air quality in Europe 2022. https://doi.org/10.2800/488115. HTML - TH-AL-22-011-EN-Q - ISBN 978-92-9480-515-7 - ISSN 1977-8449 -.

Emmons, L.K., Walters, S., Hess, P.G., Lamarque, J.-F., Pfister, G.G., Fillmore, D., Granier, C., Guenther, A., Kinnison, D., Laepple, T., Orlando, J., Tie, X., Tyndall, G., Wiedinmyer, C., Baughcum, S.L., Kloster, S., 2010. Description and evaluation of the model for ozone and related chemical Tracers, version 4 (MOZART-4). Geosci. Model Dev. (GMD) 3, 43–67. https://doi.org/10.5194/gmd-3-43-2010.

Georgiou, G.K., Christoudias, T., Proestos, Y., Kushta, J., Hadjinicolaou, P., Lelieveld, J., 2018. Air quality modelling in the summer over the eastern Mediterranean using WRF-Chem: chemistry and aerosol mechanism intercomparison. Atmos. Chem. Phys. 18, 1555–1571. https://doi.org/10.5194/acp-18-1555-2018.

Grell, G.A., Peckham, S.E., Schmitz, R., McKeen, S.A., Frost, G., Skamarock, W.C., Eder, B., 2005. Fully coupled "online" chemistry within the WRF model. Atmos. Environ. 39, 6957–6975. https://doi.org/10.1016/j.atmosenv.2005.04.027.

Guenther, A., Karl, T., Harley, P., Wiedinmyer, C., Palmer, P.I., Geron, C., 2006. Estimates of global terrestrial isoprene emissions using MEGAN (model of emissions of gases and aerosols from nature). Atmos. Chem. Phys. 6, 3181–3210. https://doi.org/10.5194/acp-6-3181-2006.

Guenther, A.B., Jiang, X., Heald, C.L., Sakulyanontvittaya, T., Duhl, T., Emmons, L.K., Wang, X., 2012. The Model of Emissions of Gases and Aerosols from Nature version 2.1 (MEGAN2.1): an extended and updated framework for modeling biogenic emissions. Geosci. Model Dev. (GMD) 5, 1471–1492. https://doi.org/10.5194/gmd-5-1471-2012.

Hardacre, C., Wild, O., Emberson, L., 2015. An evaluation of ozone dry deposition in global scale chemistry climate models. Atmos. Chem. Phys. 15, 6419–6436. https://doi.org/10.5194/acp-15-6419-2015.

Hersbach, H., Bell, B., Berrisford, P., Hirahara, S., Horányi, A., Muñoz-Sabater, J., Nicolas, J., Peubey, C., Radu, R., Schepers, D., Simmons, A., Soci, C., Abdalla, S., Abellan, X., Balsamo, G., Bechtold, P., Biavati, G., Bidlot, J., Bonavita, M., De Chiara, G., Dahlgren, P., Dee, D., Diamantakis, M., Dragani, R., Flemming, J., Forbes, R., Fuentes, M., Geer, A., Haimberger, L., Healy, S., Hogan, R.J., Hólm, E., Janisková, M., Keeley, S., Laloyaux, P., Lopez, P., Lupu, C., Radnoti, G., de Rosnay, P., Rozum, I., Vamborg, F., Villaume, S., Thépaut, J.N., 2020. The ERA5 global reanalysis. Q. J. Roy. Meteorol. Soc. 146, 1999–2049. https://doi.org/10.1002/qj.3803.

Hu, X.M., Klein, P.M., Xue, M., 2013. Evaluation of the updated YSU planetary boundary layer scheme within WRF for wind resource and air quality assessments. J. Geophys. Res. Atmos. 118 (10), 490. https://doi.org/10.1002/jgrd.50823, 10, 505.

Iungman, T., Cirach, M., Marando, F., Pereira Barboza, E., Khomenko, S., Masselot, P., Quijal-Zamorano, M., Mueller, N., Gasparrini, A., Urquiza, J., Heris, M., Thondoo, M., Nieuwenhuijsen, M., 2023. Cooling cities through urban green infrastructure: a health impact assessment of European cities. Lancet 401 (10376), 577–589. https://doi.org/10.1016/S0140-6736(22)02585-5. ISSN 0140-6736.

Karlický, J., Huszár, P., Halenka, T., 2017. Validation of gas phase chemistry in the WRF-Chem model over Europe. Adv. Sci. Res. 14, 181–186. https://doi.org/10.5194/asr-14-181-2017.

Katragkou, E., García-Díez, M., Vautard, R., Sobolowski, S., Zanis, P., Alexandri, G., Cardoso, R.M., Colette, A., Fernandez, J., Gobiet, A., Goergen, K., Karacostas, T., Knist, S., Mayer, S., Soares, P.M.M., Pytharoulis, I., Tegoulias, I., Tsikerdekis, A., Jacob, D., 2015. Regional climate hindcast simulations within EURO-CORDEX: evaluation of a WRF multi-physics ensemble. Geosci. Model Dev. (GMD) 8, 603–618. https://doi.org/10.5194/gmd-8-603-2015.

Kondo, M., Mueller, N., Locke, D., Howat, J., Rojas-Rueda, D., Schinasi, L., Gascon, M., J Nieuwenhuijsen, M., 2020. Health impact assessment of Philadelphia's 2025 tree canopy cover goals. Lancet Planet. Health 4 (4), e149–e157. https://doi.org/10.1016/S2542-5196(20)30058-9. ISSN 2542-5196.

Li, J., Miao, C., Zhang, G., Fang, Y.-H., Shangguan, W., Niu, G.-Y., 2022. Global evaluation of the Noah-MP land surface model and suggestions for selecting

parameterization schemes. J. Geophys. Res. Atmos. 127, e2021JD035753 https://doi.org/10.1029/2021JD035753.

López-Noreña, A.I., Berná, L., Tames, F., Millán, E., Puliafito, S.E., Fernandez, R.P., 2022. Influence of emission inventory resolution on the modeled spatio-temporal distribution of air pollutants in Buenos Aires, Argentina, using WRF-Chem. Atmos. Environ. 269, 118839 https://doi.org/10.1016/j.atmosenv.2021.118839. ISSN 1352-2310.

Ma, N., Niu, G.-Y., Xia, Y., Cai, X., Zhang, Y., Ma, Y., Fang, Y., 2017. A systematic evaluation of Noah-MP in simulating land-atmosphere energy, water, and carbon exchanges over the continental United States. J. Geophys. Res. Atmos. 122 https://doi.org/10.1002/2017JD027597, 12,245–12,268.

Malley, C.S., Heal, M.R., Mills, G., Braban, C.F., 2015. Trends and drivers of ozone human health and vegetation impact metrics from UK EMEP supersite measurements (1990–2013). Atmos. Chem. Phys. 15, 4025–4042. https://doi.org/10.5194/acp-15-4025-2015.

Manzini, J., Hoshika, Y., Carrari, E., Sicard, P., Watanabe, M., Tanaka, R., Badea, O., Paolo, F., Nicese, F.P., Ferrini, F., Paoletti, E., 2023. FlorTree: a unifying modelling framework for estimating the species-specific pollution removal by individual trees and shrubs. Urban For. Urban Green. 85, 127967 https://doi.org/10.1016/j.ufug.2023.127967. ISSN 1618-8667.

Martinez, Beatriz, Gilabert, M.A., Sánchez-Ruiz, Sergio, Campos-Taberner, Manuel, García-Haro, Javier, Bruemmer, Christian, Carrara, Arnaud, Feig, Gregor, Grünwald, Thomas, Mammarella, Ivan, Tagesson, Torbern, 2019. Evaluation of the LSA-SAF gross primary production product derived from SEVIRI/MSG data (MGPP). ISPRS J. Photogrammetry Remote Sens. 159, 220–236. https://doi.org/10.1016/j.isprsjprs.2019.11.010.

Masuoka, E., Albert, J.F., Wolfe, R.E., Frederick, P., 1998. Key characteristics of MODIS data products. Geoscience and Remote Sensing, IEEE Transactions on 36, 1313–1323. https://doi.org/10.1109/36.701081.

Menon, S., 2004. Current uncertainties in assessing aerosol effects on climate. Annu. Rev. Environ. Resour. 29, 1–30. https://doi.org/10.1146/annurev.energy.29.063003.132549.

Mircea, M., Borge, R., Finardi, S., Briganti, G., Russo, F., de la Paz, D., D'Isidoro, M., Cremona, G., Villani, M.G., Cappelletti, A., et al., 2023. The role of vegetation on urban atmosphere of three European cities. Part 2: evaluation of vegetation impact on air pollutant concentrations and depositions. Forests 14, 1255. https://doi.org/10.3390/f14061255.

Mlawer, E.J., Taubman, S.J., Brown, P.D., Iacono, M.J., Clough, S.A., 1997. Radiative transfer for inhomogeneous atmospheres: RRTM, a validated correlated-k model for the longwave. J. Geophys. Res. Atmos. 102, 16663–16682.

Monks, P.S., Archibald, A.T., Colette, A., Cooper, O., Coyle, M., Derwent, R., Fowler, D., Granier, C., Law, K.S., Mills, G.E., Stevenson, D.S., Tarasova, O., Thouret, V., von Schneidemesser, E., Sommariva, R., Wild, O., Williams, M.L., 2015. Tropospheric ozone and its precursors from the urban to the global scale from air quality to short-lived climate forcer. Atmos. Chem. Phys. 15, 8889–8973. https://doi.org/10.5194/acp-15-8889-2015.

Mooney, P.A., Mulligan, F.J., Fealy, R., 2013. Evaluation of the sensitivity of the weather research and forecasting model to parameterization schemes for regional climates of europe over the period 1990–95. J. Climate 26, 1002–1017.

Muñoz-Sabater, J., Dutra, E., Agustí-Panareda, A., Albergel, C., Arduini, G., Balsamo, G., Boussetta, S., Choulga, M., Harrigan, S., Hersbach, H., Martens, B., Miralles, D.G., Piles, M., Rodríguez-Fernández, N.J., Zsoter, E., Buontempo, C., Thépaut, J.-N., 2021. ERA5-Land: a state-of-the-art global reanalysis dataset for land applications. Earth Syst. Sci. Data 13, 4349–4383. https://doi.org/10.5194/essd-13-4349-2021.

Nidzgorska-Lencewicz, J., Czarnecka, M., 2020. Thermal inversion and particulate matter concentration in wrocław in winter season. Atmosphere 11, 1351. https://doi.org/10.3390/atmos11121351.

Paoletti, E., De Marco, A., Racalbuto, S., 2007. Why should we calculate complex indices of ozone exposure? Results from mediterranean background sites. Environ. Monit. Assess. 128, 19–30.

Paoletti, E., Alivernini, A., Anav, A., Badea, O., Carrari, E., Chivulescu, S., Conte, A., Ciriani, M.L., Dalstein-Richier, L., De Marco, A., Fares, S., Fasano, G., Giovannelli, A., Lazzara, M., Leca, S., Materassi, A., Moretti, V., Pitar, D., Popa, I., Sabatini, F., Salvati, L., Sicard, P., Sorgi, T., Hoshika, Y., 2019. Toward stomatal–flux based forest protection against ozone: the MOTTLES approach. Sci. Total Environ. 691, 516–527. https://doi.org/10.1016/j.scitotenv.2019.06.525. ISSN 0048-9697.

Pastorello, G., Trotta, C., Canfora, E., et al., 2020. The FLUXNET2015 dataset and the ONEFlux processing pipeline for eddy covariance data. Sci. Data 7, 225. https://doi.org/10.1038/s41597-020-0534-3.

Peng, J., Wu, C., Zhang, X., Ju, W., Wang, X., Lu, L., Liu, Y., 2021. Incorporating water availability into autumn phenological model improved China's terrestrial gross primary productivity (GPP) simulation. Environ. Res. Lett. 16, 094012 https://doi.org/10.1088/1748-9326/ac1a3b.

Perrino, C., Tofful, L., Dalla Torre, S., Sargolini, T., Canepari, S., 2019. Biomass burning contribution to PM10 concentration in Rome (Italy): seasonal, daily and two-hourly variations. Chemosphere 222, 839–848. https://doi.org/10.1016/j.chemosphere.2019.02.019. ISSN 0045-6535.

Petritoli, A., Bonasoni, P., Kaiser-Weiss, A., Schaub, D., Fortezza, F., 2003. Nitrogen Dioxide Pollution in the Po Basin: a Quantitative Analysis Based on Ground-Based and Satellite Measurements.

Pineda, N., Jorba, O., Jorge, J., Baldasano, J., 2004. Using NOAA AVHRR and SPOT VGT data to estimate surface parameters: application to a mesoscale meteorological model. International Journal of Remote Sensing - INT J REMOTE SENS 25, 129–143. https://doi.org/10.1080/0143116031000115201.

Ryu, Y.-H., Hodzic, A., Barre, J., Descombes, G., Minnis, P., 2018. Quantifying errors in surface ozone predictions associated with clouds over the CONUS: a WRF-Chem modeling study using satellite cloud retrievals. Atmos. Chem. Phys. 18, 7509–7525. https://doi.org/10.5194/acp-18-7509-2018.

Schwaab, J., Meier, R., Mussetti, G., et al., 2021. The role of urban trees in reducing land surface temperatures in European cities. Nat. Commun. 12, 6763. https://doi.org/10.1038/s41467-021-26768-w.

Sicard, P., Serra, R., Rossello, P., 2016. Spatiotemporal trends in ground-level ozone concentrations and metrics in France over the time period 1999–2012. Environ. Res. 149, 122–144. https://doi.org/10.1016/j.envres.2016.05.014. ISSN 0013-9351.

Sicard, P., Hoshika, Y., Carrari, E., et al., 2021a. Testing visible ozone injury within a Light Exposed Sampling Site as a proxy for ozone risk assessment for European forests. J. For. Res. 32, 1351–1359. https://doi.org/10.1007/s11676-021-01327-7.

Sicard, P., Agathokleous, E., De Marco, A., et al., 2021b. Urban population exposure to air pollution in Europe over the last decades. Environ. Sci. Eur. 33 (28) https://doi.org/10.1186/s12302-020-00450-2.

Sicard, P., Crippa, P., De Marco, A., Castruccio, S., Giani, P., Cuesta, J., Paoletti, E., Feng, Z., Anav, A., 2021c. High spatial resolution WRF-Chem model over Asia: physics and chemistry evaluation. Atmos. Environ. 244, 118004 https://doi.org/10.1016/j.atmosenv.2020.118004. ISSN 1352-2310.

Sicard, P., Agathokleous, E., Anenberg, S.C., De Marco, A., Paoletti, E., Calatayud, V., 2023a. Trends in urban air pollution over the last two decades: a global perspective. Sci. Total Environ. 858 (Part 2), 160064 https://doi.org/10.1016/j.scitotenv.2022.160064. ISSN 0048-9697.

Sicard, P., Coulibaly, F., Lameiro, M., Araminiene, V., De Marco, A., Sorrentino, B., Anav, A., Manzini, J., Hoshika, Y., Baesso Moura, B., Paoletti, E., 2023b. Object-based classification of urban plant species from very high-resolution satellite imagery. Urban For. Urban Green. 81, 127866 https://doi.org/10.1016/j.ufug.2023.127866. ISSN 1618-8667.

Soulie, A., Granier, C., Darras, S., Zilbermann, N., Doumbia, T., Guevara, M., Jalkanen, J.-P., Keita, S., Liousse, C., Crippa, M., Guizzardi, D., Hoesly, R., Smith, S., 2023. Global anthropogenic emissions (CAMS-GLOB-ANT) for the copernicus atmosphere monitoring service simulations of air quality Forecasts and reanalyses. Earth Syst. Sci. Data Discuss. [preprint]. https://doi.org/10.5194/essd-2023-306 submitted for publication.

Stern, R., Builtjes, P.J., Schaap, M., Timmermans, R., Vautard, R., Hodzic, A., Memmesheimer, M., Feldmann, H., Renner, E., Wolke, R., Kerschbaumer, A., 2008. A model inter-comparison study focussing on episodes with elevated PM10 concentrations. Atmos. Environ. 42, 4567–4588.

Sun, S., Tai, A.P.K., Yung, D.H.Y., Wong, A.Y.H., Ducker, J.A., Holmes, C.D., 2022. Influence of plant ecophysiology on ozone dry deposition: comparing between multiplicative and photosynthesis-based dry deposition schemes and their responses to rising CO2 level. Biogeosciences 19, 1753–1776. https://doi.org/10.5194/bg-19-1753-2022.

Terrenoire, E., Bessagnet, B., Rouïl, L., Tognet, F., Pirovano, G., Létinois, L., Beauchamp, M., Colette, A., Thunis, P., Amann, M., Menut, L., 2015. High-resolution air quality simulation over Europe with the chemistry transport model CHIMERE. Geosci. Model Dev. (GMD) 8, 21–42. https://doi.org/10.5194/gmd-8-21-2015.

Tilmes, S., Lamarque, J.-F., Emmons, L.K., Kinnison, D.E., Ma, P.-L., Liu, X., Ghan, S., Bardeen, C., Arnold, S., Deeter, M., Vitt, F., Ryerson, T., Elkins, J.W., Moore, F., Spackman, J.R., Val Martin, M., 2015. Description and evaluation of tropospheric chemistry and aerosols in the community Earth system model (CESM1.2). Geosci. Model Dev. (GMD) 8, 1395–1426. https://doi.org/10.5194/gmd-8-1395-2015.

Tuccella, P., Curci, G., Visconti, G., Bessagnet, B., Menut, L., Park, R.J., 2012. Modeling of gas and aerosol with WRF/Chem over Europe: evaluation and sensitivity study. J. Geophys. Res. 117, D03303 https://doi.org/10.1029/2011JD016302.

Wang, L., Zhu, H., Lin, A., Zou, L., Qin, W., Du, Q., 2017. Evaluation of the latest MODIS GPP products across multiple biomes using global eddy covariance flux data. Rem. Sens. 9, 418. https://doi.org/10.3390/rs9050418.

Wesely, M.L., Hicks, B.B., 2000. A review of the current status of knowledge on dry deposition. Atmos. Environ. 34 (Issues 12–14), 2261–2282. https://doi.org/10.1016/S1352-2310(99)00467-7. ISSN 1352-2310.

Wiedinmyer, C., Akagi, S.K., Yokelson, R.J., Emmons, L.K., Al-Saadi, J.A., Orlando, J.J., Soja, A.J., 2011. The fire inventory from NCAR (FINN): a high resolution global model to estimate the emissions from open burning. Geosci. Model Dev. (GMD) 4. https://doi.org/10.5194/gmd-4-625-2011.

Wiedinmyer, C., Kimura, Y., McDonald-Buller, E.C., Emmons, L.K., Buchholz, R.R., Tang, W., Seto, K., Joseph, M.B., Barsanti, K.C., Carlton, A.G., Yokelson, R., 2023. The Fire Inventory from NCAR version 2.5: an updated global fire emissions model for climate and chemistry applications. Geosci. Model Dev. (GMD) 16, 3873–3891. https://doi.org/10.5194/gmd-16-3873-2023.

Wilson, R.C., Fleming, Z.L., Monks, P.S., Clain, G., Henne, S., Konovalov, I.B., Szopa, S., Menut, L., 2012. Have primary emission reduction measures reduced ozone across Europe? An analysis of European rural background ozone trends 1996–2005. Atmos. Chem. Phys. 12, 437–454. https://doi.org/10.5194/acp-12-437-2012.

World Health Organization, 2021. WHO Global Air Quality Guidelines: Particulate Matter (PM2.5 and PM10), Ozone, Nitrogen Dioxide, Sulfur Dioxide and Carbon Monoxide. World Health Organization. https://apps.who.int/iris/handle/10665/345329.

World Health Organization Regional Office for Europe, 2013. Health Risks of Air Pollution in Europe—HRAPIE Project: WHO/EURO:2013-6696-46462-67326.

Wu, P., Christidis, N., Stott, P., 2013. Anthropogenic impact on Earth's hydrological cycle. Nat. Clim. Change 3, 807–810. https://doi.org/10.1038/nclimate1932.

Zaveri, R.A., Easter, R.C., Fast, J.D., Peters, L.K., 2008. Model for simulating aerosol interactions and chemistry (MOSAIC). J. Geophys. Res. 113, D13204 https://doi.org/10.1029/2007JD008782.

Zhang, Q., Jiang, X., Tong, D., et al., 2017. Transboundary health impacts of transported global air pollution and international trade. Nature 543, 705–709. https://doi.org/10.1038/nature21712.

Zhong, M., Saikawa, E., Liu, Y., Naik, V., Horowitz, L.W., Takigawa, M., Zhao, Y., Lin, N.-H., Stone, E.A., 2016. Air quality modeling with WRF-Chem v3.5 in East Asia: sensitivity to emissions and evaluation of simulated air quality. Geosci. Model Dev. (GMD) 9, 1201–1218. https://doi.org/10.5194/gmd-9-1201-2016.

Zhu, W., Zhao, C., Xie, Z., 2023. An end-to-end satellite-based GPP estimation model devoid of meteorological and land cover data. Agric. For. Meteorol. 331, 109337 https://doi.org/10.1016/j.agrformet.2023.109337. ISSN 0168-1923.